Intensified UV/TiO_2 Photocatalytic Treatment of Colored Wastewater: Acid Orange 10 Removal in Closed and Semi-Closed Reactors

Sarah CHAOUCHI[1*], Salima BENDEBANE[1]

[1]National Higher School of Technology and Engineering, Laboratory L3M, 23005, Annaba, Algeria

*Corresponding Author: Sarah CHAOUCHI

E-mail: s.chaouchi@ensti-annaba.dz, tel: +213 661 891 031

Graphical abstract

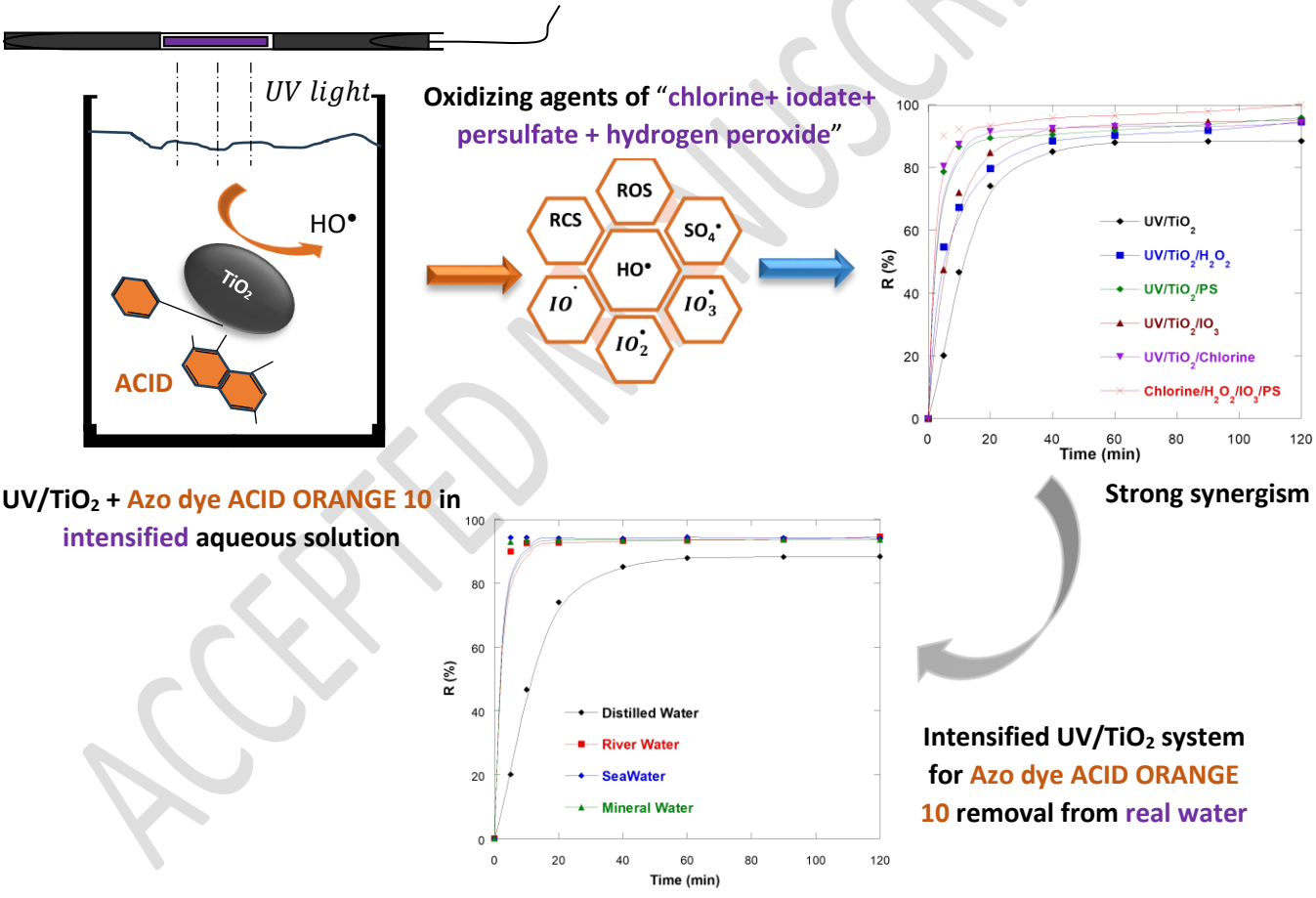

Abstract

The treatment of wastewater containing synthetic dyes represents an environmental challenge due to their complex molecular structures and high stability. This study investigates the heterogeneous photocatalytic degradation of Acid Orange 10 (AO10), an azo dye widely used in the textile industry, using titanium dioxide (TiO_2, Degussa P25) under ultraviolet (UV) irradiation in both closed and semi-closed photoreactor configurations.

Parametric optimization revealed that optimal degradation was achieved at pH 6.5, 25 °C, and 0.1 g/L TiO_2 for an initial dye concentration of 10 mg/L, reaching 88% removal efficiency after 120 min in the UV/TiO_2 system.

Process intensification through the addition of oxidizing agents (H_2O_2, $K_2S_2O_8$, Cl^-, and IO_3^-) significantly enhanced degradation performance. Among all tested systems, UV/TiO_2/IO_3^- exhibited the most remarkable enhancement, achieving 97% removal in 120 min, while the combined UV/TiO_2/IO_3^-/PS system achieved 97% removal in only 5 minutes, attributed to the synergistic generation of multiple reactive radicals (•OH, $SO_4^{\bullet-}$, and IO_3•).

Kinetic analysis confirmed that the degradation follows pseudo-first-order kinetics with excellent linearity ($R^2 \geq 0.99$), with apparent rate constants increasing proportionally with oxidant addition.

Real matrix validation using river water, seawater, and mineral water confirmed the robustness of the process, maintaining >90% degradation efficiency despite the presence of interfering ions. These findings demonstrate that TiO_2-based photocatalysis, intensified with oxidizing agents, represents an efficient and sustainable approach for treating dye-polluted effluents.

Keywords: TiO_2 photocatalysis; Acid Orange 10; Advanced Oxidation Processes; UV irradiation; Kinetics; Wastewater treatment.

1. Introduction

The global textile industry generates approximately 2.8 million tons of synthetic dyes annually, with an estimated 10-15% discharged into aquatic environments without adequate treatment (Kumar et al., 2023). Azo dyes, representing 60-70% of all textile dyes, exhibit particularly high persistence due to

their stable –N=N– bonds (bond dissociation energy ≈ 250-270 kJ/mol), which resist conventional biological treatment methods that typically achieve only 10-30% color removal.

Synthetic dyes represent a major class of persistent organic pollutants, particularly in textile and paper factories. Their excessive release into aquatic environments cause severe ecological and health hazards due to the high toxicity, color persistence, and limited biodegradability (S. Abha et al. 2018, R. Ahmad *et al.* 2016). Among these, azo dyes are the largest group used with 60%–70% from the presented synthetic species in the textile industry (I. Oller et al. 2011).

The World Health Organization (WHO) estimates that approximately 80% of diseases in developing countries are waterborne, emphasizing the necessity of efficient wastewater purification (K. González-Labrada *et al* 2020).

Conventional treatment techniques show limited effectiveness for azo dye removal. Biological degradation methods typically achieve only 10-30% color removal due to the resistance of azo bonds to microbial oxidation (A. El-Ghenymy *et al* 2022). While adsorption methods can achieve higher removal efficiencies (60-90%), they merely transfer pollutants to another phase without destruction, generating secondary waste (saturated adsorbents) that requires disposal or regeneration. Coagulation-flocculation processes also suffer from incomplete color removal and sludge generation issues. These limitations underscore the need for destructive treatment methods such as advanced oxidation processes that achieve complete mineralization (H. Suty et al. 2021). AOPs rely on the generation of highly reactive oxidative species in sufficient amount, including hydroxyl radicals ($OH^{\bullet}$, $E° = 2.8$ eV) (H.J. Wang et al. 2025, M. Dai et al. 2024), oxygen atoms (L. Peng et al. 2024), oxygen molecules (Z. Zhu et al. 2022), which non-selectively drive the decomposition of organic pollutants into inoffensive byproducts, CO_2, H_2O, and inorganic ions (H. Suty et al. 2021). photocatalytic oxidation classified as a cleaner and greener technology for azo dye degradation over the past decade (S. Li et al. 2023).

Advanced Oxidation Processes (AOPs), particularly photocatalysis, offer significant advantages over conventional methods for azo dye treatment. Unlike adsorption or coagulation, photocatalysis achieves complete mineralization rather than phase transfer, eliminating secondary waste generation. Compared to biological treatment, photocatalytic processes are not inhibited by toxic or recalcitrant compounds and operate effectively at high dye concentrations. Recent studies have demonstrated that photocatalytic

systems achieve superior removal efficiencies (>90%) compared to biological treatment (10-30%), activated carbon adsorption (60-80%), and electrocoagulation (50-70%) for azo dyes (Yudha Gusti Wibowo et al. 2025). Furthermore, photocatalysis generates powerful oxidizing species (•OH, E° = 2.8 V) that non-selectively attack organic pollutants, ensuring complete degradation of complex aromatic structures. The process operates at ambient temperature and pressure, requires no chemical addition (beyond the recyclable photocatalyst), and can utilize solar energy, offering both environmental and economic advantages for sustainable wastewater treatment (A. Dari Jaafar et al, 2024)

Photocatalytic advanced oxidation processes (P-AOPs), particularly using TiO_2 as a semiconductor catalyst with a wide band gap (3.2 eV), is one of the most promising AOPs due to its high photoactivity, low cost, and chemical stability (M.R. Hoffmann et al. 2022, M. Samadi et al. 2016).

The basic mechanism of photocatalytic starts with light absorption by the photocatalyst (TiO_2 absorbs UV radiation < 380 nm), generating electron-hole pairs that initiate redox reactions. The adsorption of the dye compounds onto the photocatalyst surface on which oxidative processes occur, leading to pollutant mineralization (N. Guettai et al. 2005). The reactions responsible for the photocatalytic dye degradation can be summarized as follows:

$$h\nu + Photocatalyst\ (TiO_2) \rightarrow h^+(TiO_2) + e^- \quad (1)$$

$$h^+\ (TiO_2) + OH^- \rightarrow OH^{\cdot} \quad (2)$$

$$O_2 + e^- \rightarrow O_2^{-\cdot} \quad (3)$$

$$4\ O_2^{-\cdot} + 2H_2O \rightarrow 4OH^{\cdot} + 3\ O_2 \quad (4)$$

$$OH^{\cdot} + dye\ contaminants \rightarrow CO_2 + H_2O \quad (5)$$

Several studies have reported TiO_2/UV systems for dye degradation, yet their performance is limited by factors such as catalyst aggregation, electron-hole recombination, and incomplete mineralization (Y. Zhao et al. 2020, S. Karuppaiah *et al.*2019). Photocatalytic process intensification involves strong oxidizing agents in addition to •OH, such as persulfate, hydrogen peroxide, periodate and chlorine, can significantly improve efficiency by generating additional radicals (G. V. Buxton et al. 1985, F. Zaviska et al. 2003).

persulfate addition to photocatalysis can lead to the generation of sulfate radicals ($SO_4^{\bullet-}$) (Q. Yang et al. 2019). The photoactivation of periodate generate iodate ions (IO_3^-), hydrogen peroxide (H_2O_2), oxygen

(O_2), and ozone (O_3). In the same system, highly reactive brief radicals as iodyl ($IO_3^{\cdot}$), periodyl ($IO_4^{\cdot}$), hydroxyl (·OH), are also produced again enhancing the oxidation of azo dye (X. Zhang et al. 2021, M. L. Djaballah et al. 2021).

In the UV/chlorine oxidation process (at 254 nm irradiation), hydroxyl radicals and several varieties of oxidants called reactive chlorine species (RCS) could be created ($Cl^{\bullet}$, $ClO^{\bullet}$, and $Cl_2^{\bullet}$) (Z. Lu et al. 2022). These species are mainly responsible for the degradation of pollutants.

In addition, extra of •OH can be formed too by directly photolysis of water using 185 nm radiation (L. Furatian et al. 2018).

This work investigates the photocatalytic degradation of Acid Orange 10 (ACID ORANGE 10) under UV irradiation in closed and semi-closed reactors using TiO_2 as a catalyst. The study systematically examines the effects of process variables (pH, temperature, catalyst loading, and initial concentration) and explores process intensification through oxidant addition. Kinetic modeling and experiments in real water matrices provide a comprehensive understanding of the system's performance and practical potential for wastewater treatment.

2. Materials and Methods

2.1. Chemicals and Solutions

All reagents were of analytical grade and used without further purification. Acid Orange 10 (ACID ORANGE 10) was selected as a model pollutant from Sigma-Aldrich, with CAS number: 1936-15-8, and purity: ≥85%. specification of the ACID ORANGE 10 is presented in Table 1.

Table 1. Specification of Acid Orange 10

Chemical name	**Acid Orange 10**
Molecular mass (g/mol)	452.36
Maximum absorption wavelength	475 nm
Molecular formula	$C_{16}H_{10}N_2Na_2O_7S_2$
Chemical Structure	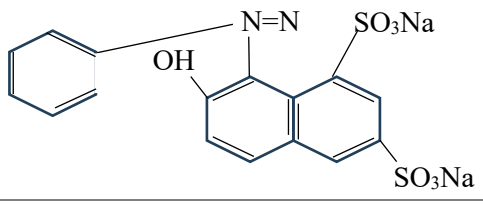

The photocatalyst used was titanium dioxide (TiO_2, Degussa P25), from Evonik Industries. A white semiconductor powder with average primary particle size: 21 nm. TiO_2 composed of ~80% anatase and ~20% rutile, with a molecular mass of 79.87 g/mol, density of 4.23 g/cm, and melting point of 1843 °C, BET (Brunauer–Emmett–Teller) surface area: 50 ± 15 m²/g, and Band gap: 3.2 eV.

The oxidizing agents included potassium persulfate (K_2S_2O8, Purity ≥99%, Sigma-Aldrich, CAS 7727-21-1), potassium iodate (KIO_3, Purity ≥99%, Sigma-Aldrich, CAS 7758-05-6), hydrogen peroxide (H_2O_2, 30% solution, Merck, CAS 7722-84-1), sodium hypochlorite (NaClO, 13% active chlorine, VWR, CAS 7681-52-9), and other supporting salts (KH_2PO_4, K_2SO_4, KNO_3, K_2CrO_4, $K_4[Fe(CN)_6]\cdot 3H_2O$). with Purity ≥99%, Sigma-Aldrich.

Each oxidant was selected for its ability to generate radicals such as $SO_4^{\bullet-}$, $OH^{\bullet}$, $IO^{\bullet}$, or $Cl^{\bullet}$ under UV excitation.

Alcohols (Ethanol C_2H_5OH: Purity ≥99.8%, absolute, Sigma-Aldrich, 2-Propanol C_3H_7OH: Purity ≥99.5%, Sigma-Aldrich, and tert-Butanol C_4H_9OH: Purity ≥99%, Sigma-Aldrich) were used as radical scavengers, while Ascorbic acid $C_6H_8O_6$: Purity ≥99%, Sigma-Aldrich) served as a reducing agent in certain control tests.

All working solutions were freshly prepared in distilled water, with Conductivity <2 µS/cm, produced in-laboratory, and pH was adjusted to 6.5 ± 0.1 using 0.1 M of Sodium hydroxide (NaOH): Purity ≥98%, pellets, Merck, or Hydrochloric acid (HCl): 37%, Merck, using HANNA pH-211 meter, calibrated at pH 4, 7, and 10.

To ensure complete dispersion of the contaminants in the solution, the solution was mixed with the required amount of catalyst and magnetically spun in the dark. The UV light, located at the center of the reactor, was then turned on. An external water- cooling system was used around the reactor to maintain the temperature during the process experiments.

2.2. Photocatalytic Reactor (Closed System)

Photocatalytic experiments were conducted in a cylindrical borosilicate glass reactor with a total capacity of 500 mL and an effective working volume of 250 mL (Figure 1). The reactor had an internal

diameter of 8 cm and a height of 15 cm. Irradiation was provided by a low-pressure mercury UV lamp (λ = 254 nm, 12 W), positioned vertically at a fixed distance of 5 cm above the liquid surface to ensure uniform photon distribution. The reactor was enclosed with an aluminum shield to minimize external light interference and enhance UV reflection toward the reaction medium. The reaction temperature was maintained at 25 ± 1 °C, continuously monitored using a K-type thermocouple with an accuracy of ±0.5 °C, immersed directly in the solution. The suspension was continuously agitated using a magnetic stirrer operating at 300 rpm, equipped with a 2 cm magnetic stir bar, to ensure homogeneous dispersion of TiO_2 particles throughout the reaction medium. The initial pH was adjusted to 6.5 and measured before and after each experiment using a combined glass electrode (HANNA pH-211).

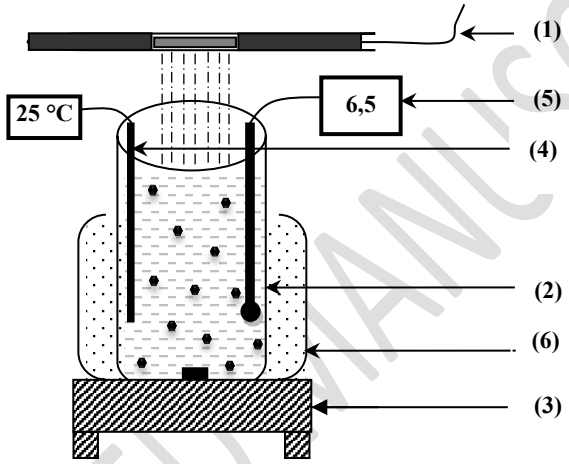

Figure 1. Experimental setup of the closed photocatalytic reactor. Components: (1) UV lamp 254 nm, 12 W, positioned 5 cm above liquid surface; (2) cylindrical borosilicate glass reactor (Ø = 8 cm, H = 15 cm, V = 250 mL); (3) magnetic stirrer (300 rpm); (4) K-type thermocouple; (5) pH meter; (6) ultrasonic transducer (40 kHz, 100 W, positioned at external bottom—used only for experiments in Figure 5). Operational conditions: [AO10] = 10 mg/L, [TiO_2] = 0.1 g/L, pH 6.5.

2.3. Semi-Closed Photocatalytic System

To enhance mass transfer and photon utilization efficiency, a semi-closed dual-reactor configuration was employed (Figure 2). The system consisted of two identical cylindrical borosilicate glass reactors, each having the same dimensions as the closed system reactor (8 cm diameter and 15 cm height), and separated by a fixed distance of 50 cm. Both reactors were equipped with cooling jackets to maintain a

constant operating temperature of 25 °C. Continuous circulation of the ACID ORANGE 10 suspension between the two reactors was ensured by a peristaltic pump (Kerlabo) operating at a constant flow rate of 100 mL/min, maintaining a total working volume of 250 mL and a TiO_2 concentration of 0.1 g/L. The system was irradiated simultaneously using two UV sources: a low-pressure mercury lamp (254 nm) and a high-power UV lamp (UVITALux, 300 W, 280–400 nm, UV-A/B range). This configuration enabled sequential exposure of the circulating suspension to different UV intensities and spectral ranges, thereby improving photocatalytic efficiency. Experiments were conducted for 120 minutes, with periodic sampling for kinetic monitoring. Figure 2. Experimental setup of the semi-closed photocatalytic system with continuous circulation between two UV-irradiated reactors. After each irradiation interval, aliquots were withdrawn and centrifuged using a REMI R-8C DX centrifuge at 4500 rpm for 30 min at 25 °C to remove suspended TiO_2 particles and avoid light scattering during UV–Vis analysis. This separation step ensured accurate determination of the residual dye concentration.

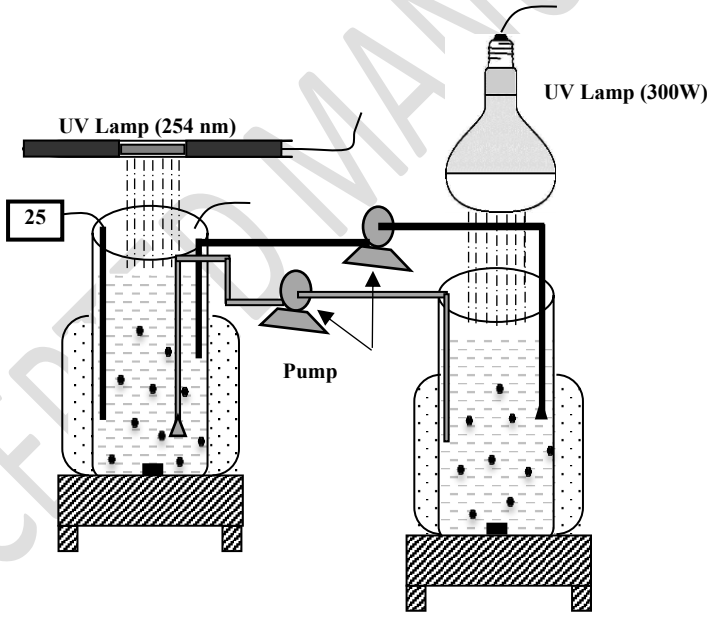

Figure 2. Experimental setup of the semi-closed photocatalytic system with continuous circulation between two UV-irradiated reactors.

2.4. Spectrophotometric Analysis

The degradation of ACID ORANGE 10 was monitored by UV-Vis spectrophotometry using a Shimadzu UV-1900i spectrophotometer equipped with 1 cm quartz cells.

Absorbance was measured at λmax = 482 nm, corresponding to the characteristic band of the azo chromophore (–N=N–) of ACID ORANGE 10.

The concentration of the dye was determined using the Beer-Lambert law, and the degradation efficiency (η) was calculated as:

$$\eta(\%) = \frac{C_0 - C_t}{C_0} \times 100 \qquad (6)$$

Where:

η = degradation efficiency (%)

C_0 = initial dye concentration (mg/L) ; C_t = dye concentration at time t (mg/L)

3. Results and Discussion

3.1. Photocatalytic degradation in the closed reactor

3.1.2. Adsorption on TiO_2

For the catalytic reaction, surface area providing adsorption sites for the substrate, and the overall rate depending on surface reactions, the physical and structural properties of those catalysts. While, photocatalysts have their own activity.

To identify the optimal conditions for dye degradation by photocatalysis and to ensure that the observed ACID ORANGE 10 removal results from oxidation rather than simple physical adsorption onto the catalyst surface, preliminary adsorption tests were carried out on TiO_2.

Initially, the adsorption of ACID ORANGE 10 onto titanium dioxide was investigated under dark conditions. A 250 mL solution containing 10 mg/L ACID ORANGE 10 and 0.1 g/L TiO_2 was magnetically stirred for one hour. The variation of the normalized concentration (C/C_0) as a function of contact time with TiO_2 is presented in Figure 3.

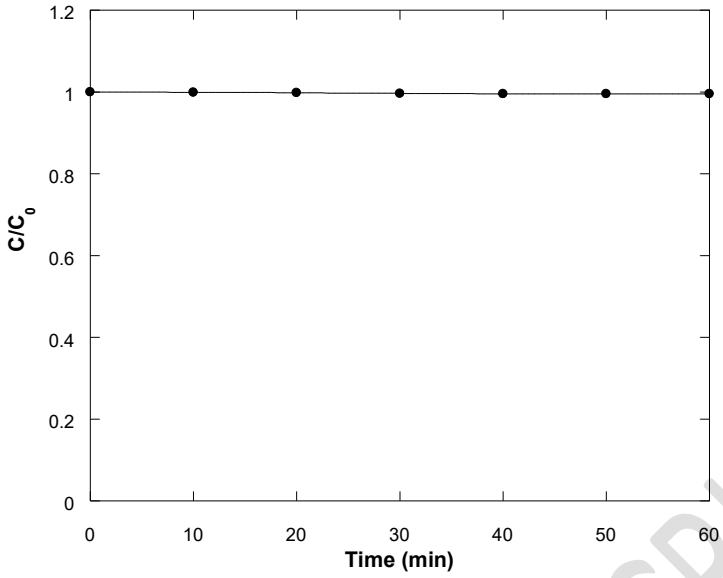

Figure 3. Adsorption kinetics of ACID ORANGE 10 on TiO_2 *([ACID ORANGE 10] = 10 mg/L; [TiO_2] = 0.1 g/L ; V = 250 mL; T = 25 °C)*

At the initial time (t = 0), $C/C_0 = 1.0$, representing the starting condition. During the first 10 minutes of contact under dark conditions, the normalized concentration decreased from 1.0 to approximately 0.96, corresponding to 4% removal by physical adsorption onto the TiO_2 surface. After this initial period, the C/C_0 value remained constant at approximately 0.96, indicating that adsorption equilibrium had been established. This equilibrium state persisted even after 60 minutes of continuous stirring, confirming that no additional adsorption occurred beyond the initial 10-minute period.

Increasing the TiO_2 mass does not necessarily lead to a higher number of adsorption sites or an improved adsorption rate (E. Vulliet et al. 2003). This behavior can be attributed to two major factors: (i) increasing the TiO_2 loading may induce pH variations in the solution, thereby altering the surface charge state of the catalyst and reducing its affinity toward the dye molecules; (ii) excessive TiO_2 concentrations promote particle agglomeration, which decreases the number of accessible active sites and consequently limits the adsorption efficiency (M. Sleiman et al. 2009, Y. Lin et al. 2009).

Previous studies have also shown that ACID ORANGE 10 exhibits weak adsorption on catalyst surfaces, with very similar adsorption constants, which explains the small amount adsorbed on TiO_2 and the

consistently low adsorption capacities reported for similar system (R. Brina et al. 1987, X. Zhang et al. 2019).

3.1.3. Direct photolysis

To assess the true efficiency of the photocatalytic process, it was essential to determine the contribution of direct photolysis to ACID ORANGE 10 degradation under the same operational conditions. For this purpose, a control experiment was conducted using a 10 mg/L ACID ORANGE 10 solution exposed to UV irradiation at 254 nm in the absence of TiO_2.

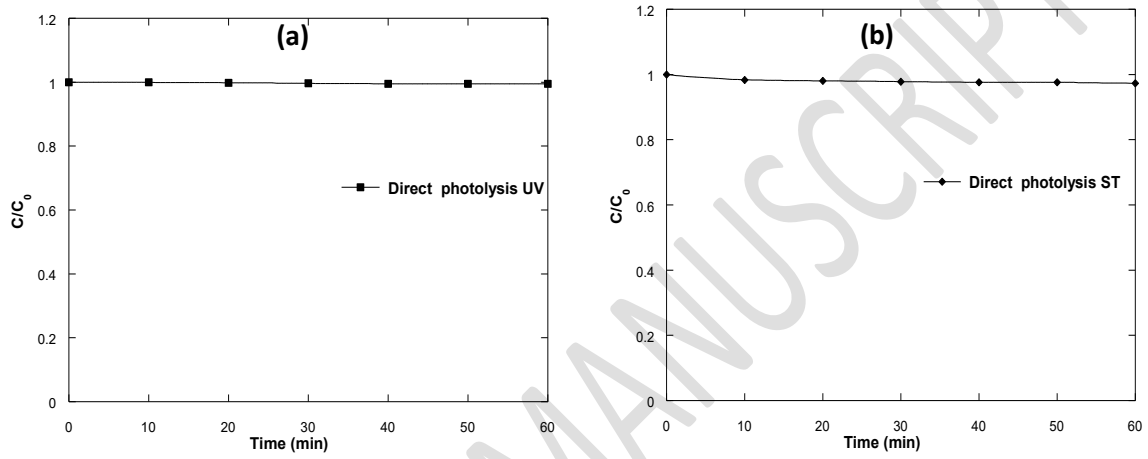

Figure 4 presents the variation of the normalized concentration (C/C_0) of ACID ORANGE 10 as a function of irradiation time under both UV (a) and simulated solar light (ST) (b). (*[ACID ORANGE 10] =10 mg/L; V = 250 mL; T = 25 °C)*

The results clearly show that ACID ORANGE 10 solution has not undergone any change during these 60 min of direct photolysis. At the end, only a 2% decrease in concentration was observed, indicating that ACID ORANGE 10 is highly stable under UV light alone. UV-Vis spectral analysis confirmed that no significant change occurred in the absorption spectra throughout the experiment.

These findings confirm that any subsequent removal of ACID ORANGE 10 in the presence of TiO_2 results from true photocatalytic oxidation rather than direct photolysis, in agreement with previous studies on azo dyes under similar UV conditions (C. Lee et al. 2023, L. Zhang et al. 2024, J. Díaz-Torres *et al.* 2022).

3.1.4. Effect of different TiO_2 activation sources (UV, US, ST)

Photocatalytic dye removal inherently light- dependent. Under different light (UV, visible, and solar lights) irradiation, the penetration of light on TiO_2 particles generate electron–hole pairs, that enhances the production of reactive oxygen species, especially $OH^{\bullet}$, which plays a central role in dye mineralization.

Combination of ultrasonic (US) waves with heterogeneous catalysts is an important strategy that led to the increase in photo-thermal catalytic activity, and controlling surface properties of catalysts (A. V. Mohod et al. 2023).

The activation of the TiO_2 semiconductor under various irradiation sources, including a 12 W UV-C lamp, a 300 W UV-A simulator lamp (ST), and ultrasonic activation (US) at low frequency were investigated. The corresponding degradation profiles of ACID ORANGE 10 are shown in Figure 5.

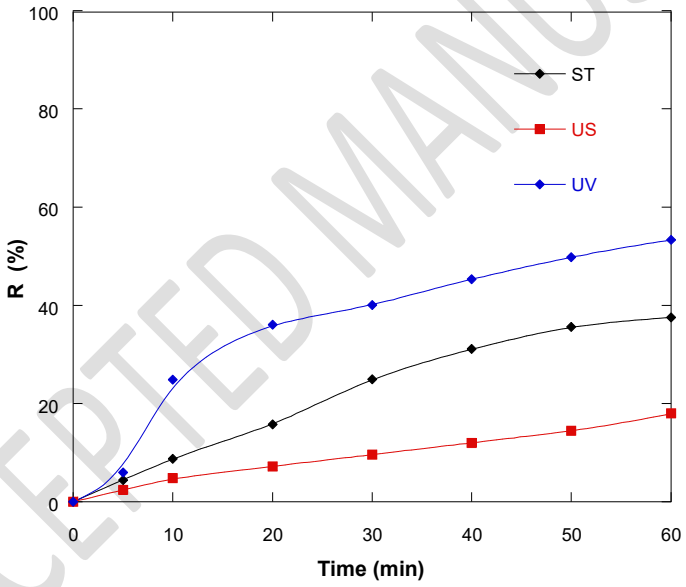

Figure 5. Degradation profiles of ACID ORANGE 10 (*[ACID ORANGE 10] = 10 mg/L; [TiO_2] = 0.1 g/L; V = 250 mL; T = 25 °C)*

The results reveal a marked influence of the irradiation source on the photocatalytic performance. Under UV-C irradiation, ACID ORANGE 10 degradation reached 52% after 60 min, compared to 36% under simulated solar light and only 17% under ultrasonic activation.

The superior performance of UV activation is attributed to the higher photon energy ($\lambda = 254$ nm), which effectively excites the TiO_2 band gap (3.2 eV) and generates a larger number of electron-hole pairs.

The moderate activity under simulated solar light is associated with the limited fraction of photons in the UV range capable of initiating photocatalytic reactions. In contrast, ultrasonic activation induced only partial degradation, due to the low increased generation of electron-hole pairs and the limited production of hydroxyl radicals, whose contribution remained minor compared with direct UV photoexcitation (C. Lee et al. 2023, L. Zhang et al. 2024, J. Díaz-Torres *et al.* 2022).

poor light absorption, and relatively small specific surface area limited generation of reactive oxygen species (ROS) and therefor prevent its catalytic performance. These results highlight the critical role of photon energy in TiO_2 activation and confirm that UV-driven processes are far more efficient for the degradation of ACID ORANGE 10 and similar azo dyes.

3.1.5. Photocatalysis and degradation spectra

Figure 6 shows the evolution of the UV-Vis absorption spectra of ACID ORANGE 10 during photocatalytic treatment under UV irradiation.

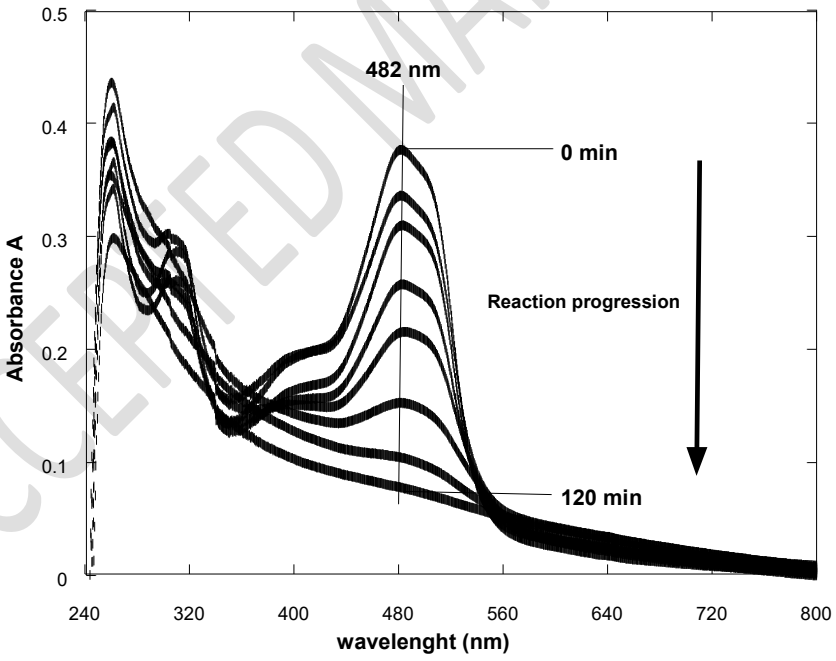

Figure 6. Evolution of the UV-Vis absorption spectra of Acid Orange 10 during photocatalytic treatment under UV irradiation in closed reactor configuration. Experimental conditions: $[AO10]_0$ = 10 mg/L; $[TiO_2]$ = 0.1 g/L; pH = 6.5; T = 25°C; V = 250 mL; UV lamp = 254 nm (12 W). Spectra recorded at 0, 15, 30, 60, 90, and 120 min.

Figure.6 displays the variations in the UV–visible spectrum of ACID ORANGE 10 dye solution over time. The dye's characteristic wavelength, 482 nm, corresponding to the π-π* transition of the azo (–N=N–) chromophore. As the irradiation time increases, this band progressively decreases in intensity and nearly disappears after 120 minutes of photocatalysis.

The gradual decrease and eventual disappearance of the 482 nm band indicate the cleavage of the azo linkage and the breakdown of the conjugated aromatic structure of ACID ORANGE 10. These spectral changes confirm that the photocatalytic process effectively decomposes the chromophoric system into smaller, non-absorbing intermediates.

The broadening and slight shift in the spectra observed during degradation can be attributed to the formation of transient aromatic intermediates, which are subsequently mineralized into low-molecular-weight species. Similar spectral behavior has been reported for other azo dyes degraded by TiO_2-based photocatalysts (C. Lee et al. 2023, L. Zhang et al. 2024, J. Díaz-Torres *et al.* 2022).

3.2. Parametric study

3.2.1. Effect of initial ACID ORANGE 10 concentration and kinetic analysis

The influence of the initial dye concentration on the photocatalytic degradation of ACID ORANGE 10 was examined in the range of 5-40 mg/L at natural pH and a constant TiO_2 loading of 0.1 g/L.

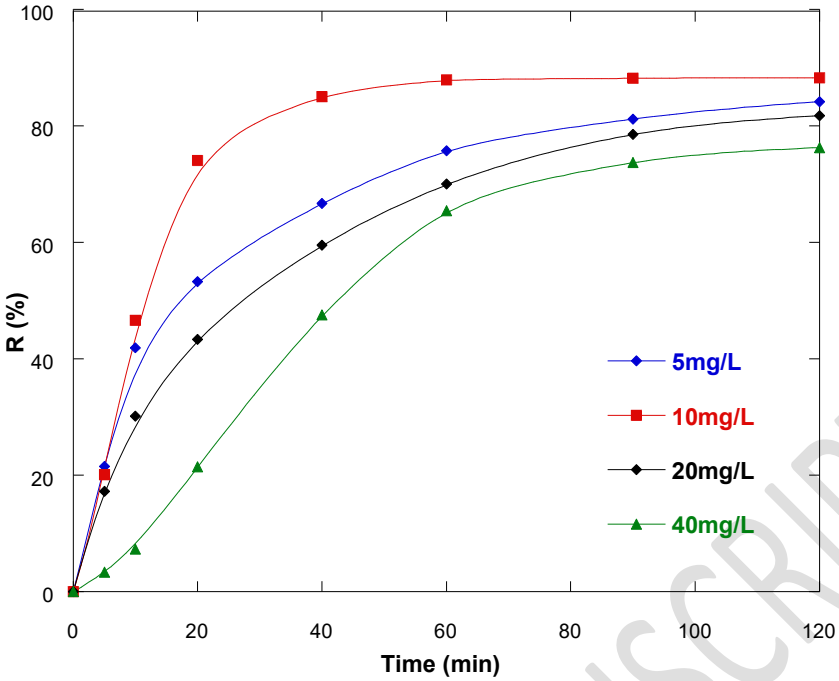

Figure 7. Effect of the initial ACID ORANGE 10 concentration *([TiO_2] = 0.1 g/L; V = 250 mL; T = 25 °C)*

As shown in Figure 7, the degradation rate decreased with increasing dye concentration under constant catalyst loading. At low concentrations (≤ 10 mg/L), almost complete elimination (88.31%) was achieved within 120 min, whereas higher concentrations resulted in slower degradation (76.27%). This behavior is attributed to photon screening as a result of the intensified concentration gradient, and the limited availability of active sites, has an inhibitory effect on the production of holes and OH radicals. Moreover, competitive reaction may occur between dye molecules and reactive species generated during the degradation, which could potentially explain the observed decrease in degradation efficiency. Furthermore, the number of radicals generated through photocatalytic process becomes insufficient relatively to the increasing number of dye molecules.

The kinetic behavior of ACID ORANGE 10 degradation was evaluated using the pseudo-first-order model:

$$r = -\frac{dC}{dt} = k_{app}C \qquad (7)$$

$$=> \ln\frac{C_0}{C} = k_{app}\, t \qquad (8)$$

Where :

r : rate of photocatalytic reaction

C : dye concentration at time t (mg/L)

C_0 = initial dye concentration (mg/L)

t : time (min)

k_{app} : the apparent rate constant (min^{-1})

The plots of $\ln\frac{C_0}{C}$ versus irradiation time (Figure 8) exhibit excellent linearity ($R^2 \geq 0.99$), confirming that ACID ORANGE 10 degradation follows pseudo-first-order kinetics.

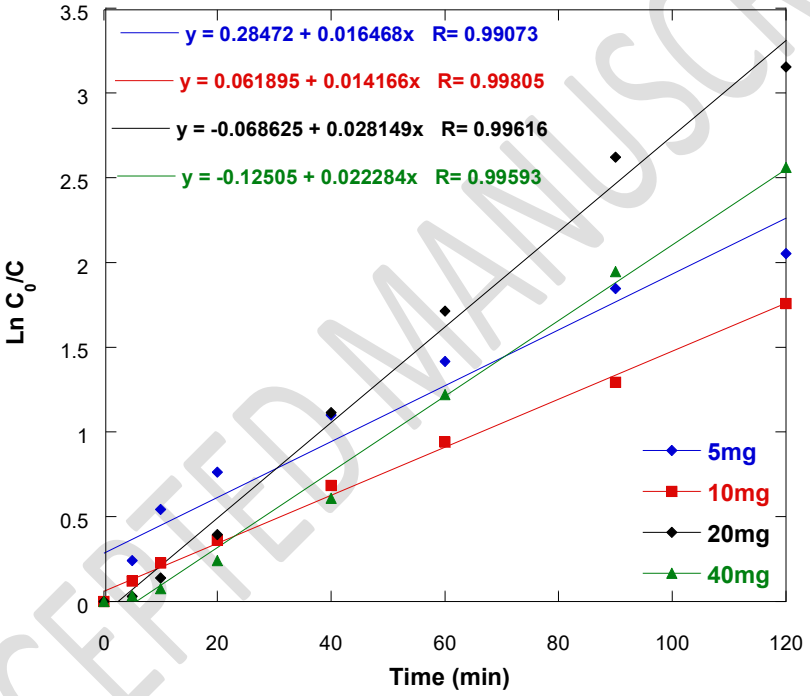

Figure 8. First-order reaction rate *([TiO_2] = 0.1 g L^{-1}; V = 250 mL; T = 25 °C)*

The apparent rate constant (k_{app}) decreases with increasing C_0, reflecting the combined effects of light attenuation and surface saturation. This trend is consistent with the Langmuir-Hinshelwood kinetic model commonly observed for TiO_2 photocatalysis (C. Lee et al. 2023, L. Zhang et al. 2024, J. Díaz-Torres *et al.* 2022).

3.2.2. Effect of TiO_2 Dosage

The influence of the catalyst mass on the photocatalytic degradation of ACID ORANGE 10 was investigated using different TiO_2 dosages: 0.01, 0.05, 0.1, 0.5, and 1 g/L.

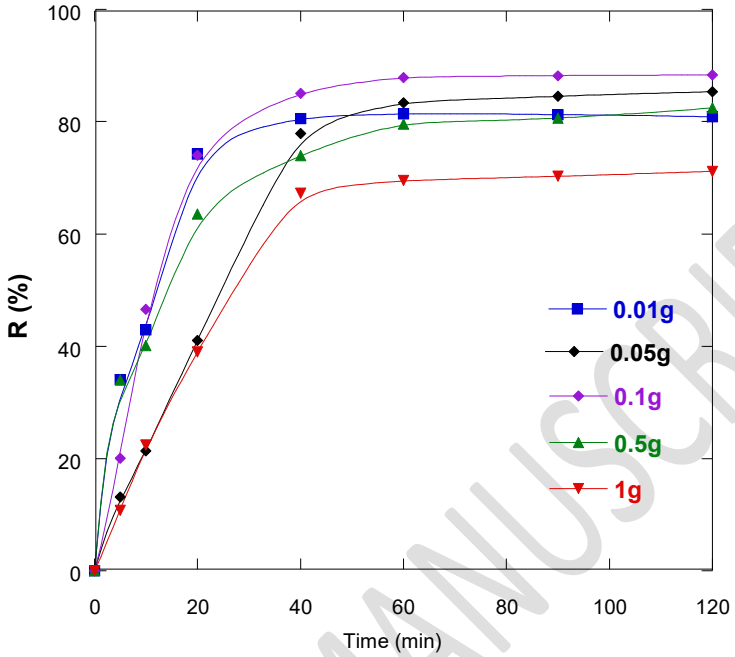

Figure 9. Effect of TiO_2 mass on the photocatalytic degradation of ACID ORANGE 10 *([ACID ORANGE 10] = 10 mg L^{-1}; V = 250 mL; T = 25 °C)*

As shown in Figure 9, the degradation rate increases with TiO_2 loading up to 0.1 g/L, beyond which the efficiency levels off. The initial rate enhancement is attributed to the larger surface area available for photon absorption and dye adsorption, resulting in the generation of more electron-hole pairs and reactive hydroxyl radicals (•OH). Hence, the more active sites, the better the catalyst performance (A, Dari et al. 2025).

However, when the TiO_2 concentration exceeds 0.1 g/L, the reaction rate no longer improves significantly and even slightly decreases. This decline is due to light scattering and both of opacity and turbidity of the suspension at higher catalyst loadings, which reduce the effective photon flux reaching the catalyst surface. Moreover, excessive particle agglomeration at high concentrations can limit the number of available active sites and hinder the diffusion of dye molecules toward the surface (C. Lee et al. 2023, L. Zhang et al. 2024, J. Díaz-Torres *et al.* 2022).

Since surface area and particle size are closely related to each other, it can empirically be stated that the smaller the particle size is, the higher is the activity of a photocatalyst. The optimal TiO_2 loading was therefore fixed at 0.1 g/L, corresponding to a balance between efficient photon utilization and minimal light attenuation. Similar optimal values have been reported in the photocatalytic degradation of other azo dyes and organic contaminants using Degussa P25 TiO_2 under comparable conditions (J. Díaz-Torres *et al.* 2022, M. R. Hoffmann et al. 2022, G. R. Peyton et al. 1974).

3.2.3. Effect of pH

The pH of the reaction medium is a crucial operational parameter in photocatalytic processes because it strongly influences the surface charge of TiO_2 and the ionization state of the dye. The photocatalytic degradation of ACID ORANGE 10 was examined at different pH values (1, 3, 6.5, 9, and 12). The pH was adjusted using HCl for acidic and NaOH for basic conditions.

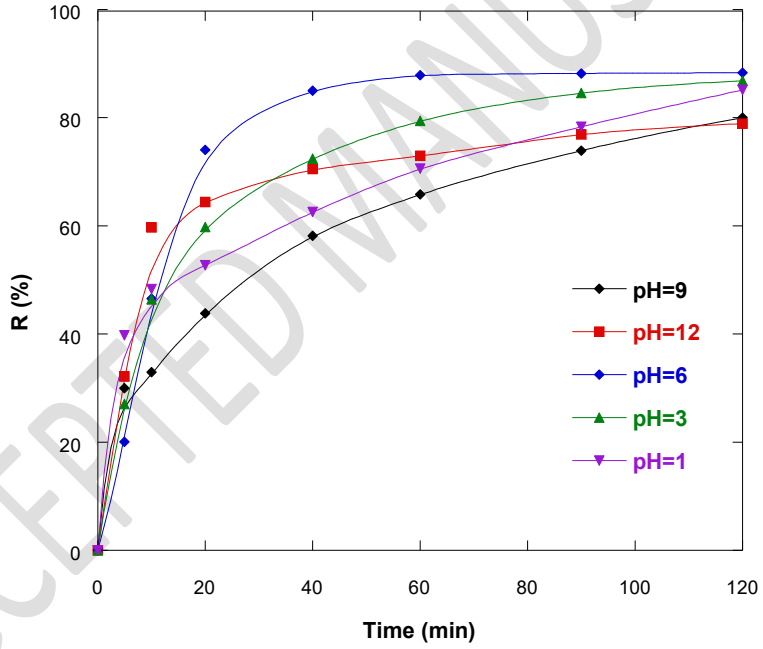

Figure 10. Effect of solution pH on the photocatalytic degradation of ACID ORANGE 10 (*[ACID ORANGE 10] = 10 mg L^{-1}; [TiO_2] = 0.1 g L^{-1}; V = 250 mL; T = 25 °C)*

As shown in Figure 10, the degradation rate was highest under mildly acidic conditions (pH 3-6), decreased at high pH, and was almost constant near neutral conditions. This behavior can be explained by electrostatic interactions between the charged TiO_2 surface and the ionic dye species. TiO_2 is amphoteric and exhibits a point of zero charge (PZC) around pH 6.8 (Degussa P25). When pH < PZC,

the catalyst surface is positively charged, favoring adsorption of anionic dyes such as ACID ORANGE 10 and enhancing degradation efficiency. Conversely, when pH > PZC, the surface becomes negatively charged, leading to electrostatic repulsion that inhibits adsorption and lowers photocatalytic activity (C. Lee et al. 2023, L. Zhang et al. 2024, J. Díaz-Torres *et al.* 2022).

The main surface reactions can be expressed as:

$$TiOH + H^+ \rightarrow TiOH_2{}^+ \quad (9)$$

$$TiOH + OH^- \rightarrow TiO^- + H_2O \quad (10)$$

Hydroxyl radicals (•OH) are generated by oxidation of water molecules trapped on the catalyst surface:

$$H_2O + h^+ \rightarrow HO^{\cdot} + H^+ \quad (11)$$

At very low pH, the adsorption of hydronium ions (H_3O^+) on TiO_2 reduces hydroxyl radical formation due to competition for active sites, slightly lowering degradation efficiency. At high pH, excess hydroxide ions (OH^-) can react with photogenerated holes, producing additional •OH radicals, but excessive negative charge on the surface limits this effect (M, Jaafar et al, 2025).

The optimal degradation of ACID ORANGE 10 was achieved under mildly acidic conditions (around pH 6), consistent with trends reported for other anionic azo dyes (J. Díaz-Torres *et al.* 2022, M. R. Hoffmann et al. 2022, G. R. Peyton et al. 1974).

3.2.4. Effect of temperature

The photocatalytic degradation of ACID ORANGE 10 was studied at different temperatures (15, 25, and 35 °C) under otherwise identical conditions.

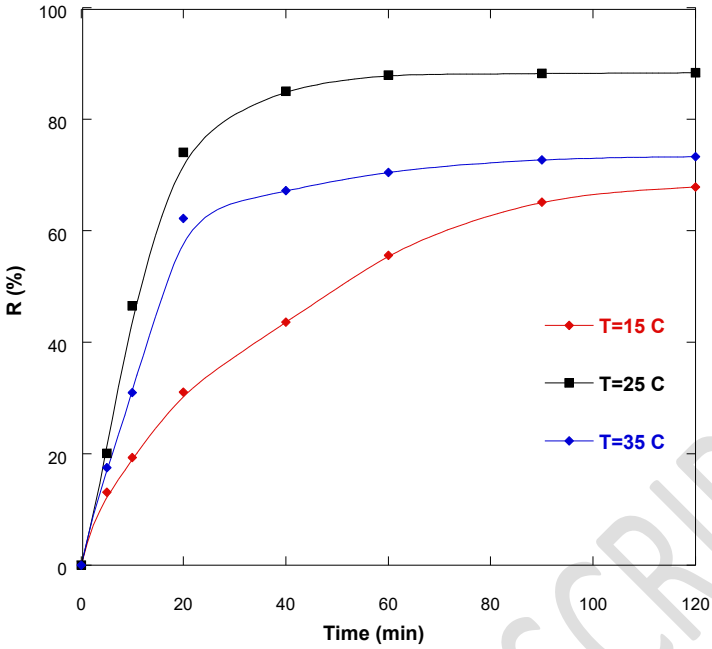

Figure 12. Effect of temperature on ACID ORANGE 10 degradation *([ACID ORANGE 10]=10 mg L^{-1}; [TiO_2]=0.1 g/L; V = 250 mL)*

As illustrated in Figure 12, temperature had a moderate effect on photocatalytic activity. The degradation efficiency increased from 67 % at 15 °C to 88 % and 84 % at 25 °C and 35 °C, respectively. This indicates that the process is only weakly temperature-dependent within the investigated range.

At lower temperatures, the reduced degradation efficiency is mainly attributed to a decrease in dye adsorption on the TiO_2 surface, which limits the formation of reactive hydroxyl radicals (•OH). The slight drop in activity observed at 35 °C can be explained by the enhanced desorption of ACID ORANGE 10 molecules and faster recombination of photogenerated electron-hole pairs at elevated temperatures.

The temperature 25 °C was identified as the most favorable operating temperature, providing a balance between sufficient adsorption of dye molecules and effective radical generation. Similar trends have been reported for other anionic dyes, confirming that photocatalytic degradation over TiO_2 is primarily governed by photochemical rather than thermal activation (C. Lee et al. 2023, L. Zhang et al. 2024, J. Díaz-Torres *et al.* 2022).

3.3. Process intensification by addition of oxidizing agents

Heterogeneous photocatalysis using TiO_2 is an efficient approach for the degradation of organic pollutants. However, its performance can be further enhanced by coupling the UV/TiO_2 system with external oxidizing substances such as persulfate ($S_2O_8^{2-}$), hydrogen peroxide (H_2O_2), hypochlorite (Cl^-/HOCl), or iodate (IO_3^-). These oxidants act as electron acceptors, suppressing charge recombination and can be reductively converted into highly reactive oxygen species (ROS) such as sulfate ($SO_4^{\bullet}$), hydroxyl ($^{\bullet}OH$), chlorine ($Cl^{\bullet}$), iodyl ($IO_3^{\bullet}$) and periodyl ($IO_4^{\bullet}$), and thereby improving degradation efficiency (S. Ahmed et al. 2010, T. Wu et al. 1998).

3.3.1. UV/TiO_2/$K_2S_2O_8$ system

Persulfate (PS) including potassium persulfate (KPS) has been investigated for wastewater remediation due to its capacity to degrade organic contaminants (I.A. Ike et al. 2028).

Persulfate ions ($S_2O_8^{2-}$) are among the most powerful oxidants in aqueous solution. Upon UV activation, they produce sulfate radicals ($SO_4^{\bullet-}$) with higher redox potential (E° = 2.6 V) and longer lifetime, and hydroxyl radicals ($^{\bullet}OH$) enabling efficient oxidation. Degradation mechanisms of sulfate radicals are based on hydrogen abstraction, addition on double bond and electron transfer, as shown in Equations (12-314):

$$S_2O_8^{2-} + e^- \rightarrow SO_4^{\bullet-} + SO_4^{2-} \quad (12)$$

$$SO_4^{2-} + H_2O \rightarrow \bullet OH + SO_4^{2-} + H^+ \quad (13)$$

$$SO_4^{\bullet-} + \bullet OH + \text{dye} \rightarrow \text{degradation products} \quad (14)$$

The UV/TiO_2/PS results were compared with those obtained by UV/TiO_2 and as expected, faster degradation was found at higher oxidant concentration. These radicals participate in hydrogen abstraction or electron-transfer reactions with organic compounds

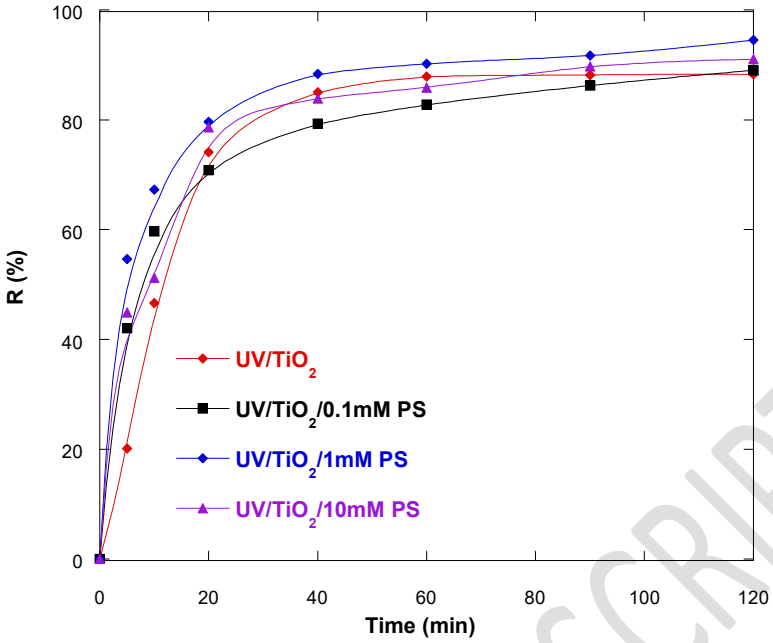

Figure 13. UV/TiO_2/$K_2S_2O_8$ degradation system

Figure 13 show the influence of persulfate dose on process efficiency. As illustrated, adding persulfate accelerated first ACID ORANGE 10 degradation compared to UV/TiO_2 alone, and then decreased with the increasing persulfate dose. The improvement is attributed to both the inhibition of electron-hole recombination and the generation of $SO_4^{\bullet-}$ radicals, which complement hydroxyl radicals in the oxidation process (F. Legrini et al. 1993).

The competitive destruction of the organic matter present in solution caused a slower dye abatement in the UV/TiO_2/PS process, probably due to the larger attack of $SO_4^{\bullet}$ than $^{\bullet}OH$.

In contrast, when the persulfate dose was high (≥1mM), no significant enhancement of removal efficiency was recorded, mostly due to the limited dosage of catalyst. However, when the excessive dosage of PS was introduced, the in situ generated $SO_4^{\bullet-}$ radicals can be captured by persulfate molecules (Eq. (15)), thereby decreasing the decontamination efficiency (Y.R. Wang et al. 2019, P. L. Hao et al. 2020).

$$SO_4^{\bullet-} + S_2O_8^{2-} \rightarrow S_2O_8^{\bullet-} + SO_4^{2-} \qquad (15)$$

3.3.2. UV/TiO_2/H_2O_2 system

Hydrogen peroxide (H_2O_2) is a commonly used oxidizing substance (E° = 0.8 V), especially valued for producing hydroxyl radicals (•OH) under UV irradiation (λ < 330 nm), in aqueous applications:

$$H_2O_2 + h\upsilon \rightarrow 2HO^{\bullet} \qquad (16)$$

The addition of H_2O_2 during UV/TiO_2 system treatment significantly improved the degradation efficiency. •OH generation increased substantially with higher H_2O_2 doses at moderate concentrations (20 mM in this study), which enhances the degradation rate (Figure 14) by scavenging conduction-band electrons and promoting charge separation:

$$H_2O_2 + e^- \rightarrow OH^- + HO^{\bullet} \qquad (17)$$

However, excessive H_2O_2 may act as a radical scavenger, reducing efficiency through reactions [28-29] such as:

$$H_2O_2 + O_2^{\bullet} \rightarrow OH^- + HO^{\bullet} + O_2 \qquad (18)$$

Therefore, using an optimal concentration is crucial for maximizing performance.

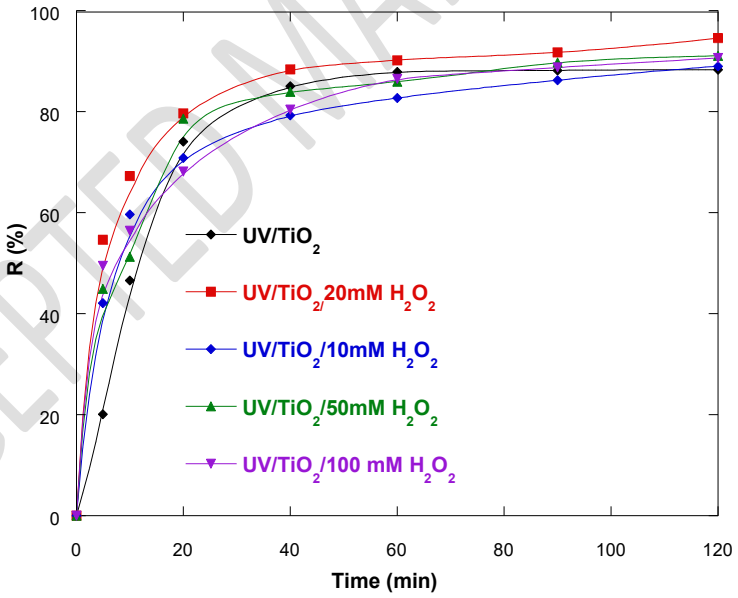

Figure 14. UV/TiO_2/H_2O_2 degradation system

3.3.3. UV/TiO_2/Cl system

In advanced oxidation processes (AOPs), UV/Cl system is related to the synergistic UV-chlorination effects generating reactive species (RCS) such as Cl•, $Cl_2^{\bullet-}$, and ClO•. These radicals are characterized

by greater redox potentials (E° =2.43 V for $Cl^{\bullet}$, E° = 2.13 V for $Cl_2^{\bullet}$ and E° = 1.5–1.8 V for $ClO^{\bullet}$, at environmentally pH values (pH 6–9).

In contrast to •OH, RCS are selective active species that can preferentially react with many rich electron organic compounds, these radicals are formed via photolysis (at 254 nm irradiation). Hypochlorous (HClO) forms $^{\bullet}OH$, $Cl^{\bullet}$ radicals, and more reactive chlorine species during HCLO photo-activation. According to the following mechanism, multiple chemical reactions comprising several reactive radicals ($Cl^{\bullet}$, $ClO^{\bullet}$, $^{\bullet}OH$, $O^{\bullet}$, $Cl_2^{\bullet}$) and non-radical intermediates/products (ClO^-, Cl^-) are described (Mohamed Larbi Djaballaha et al. 2023):

$$HClO + h\nu \rightarrow 2HO^{\bullet} + Cl^{\bullet} \qquad k = (0.81 - 6.9) \times 10^3\ s^{-1} \qquad (19)$$

$$ClO^- + h\nu \rightarrow O^{\bullet -} + Cl^{\bullet} \qquad k = (0.87 - 8.3) \times 10^3\ s^{-1} \qquad (20)$$

$$O^{\bullet -} + H_2O \leftrightarrow HO^{\bullet} + OH^- \qquad k_1 = 1.8 \times 10^6\ M^{-1}s^{-1}$$

$$k_{-1} = 1.3 \times 10^{10}\ M^{-1}s^{-1} \qquad (21)$$

$$HO^{\bullet} + HClO^{\bullet} \rightarrow ClO^{\bullet} + H_2O \qquad k = 2 \times 10^9\ M^{-1}s^{-1} \qquad (22)$$

$$HO^{\bullet} + ClO^- \rightarrow ClO^{\bullet} + OH^- \qquad k = 8.8 \times 10^9\ M^{-1}s^{-1} \qquad (23)$$

$$Cl^- + Cl^{\bullet} \leftrightarrow Cl_2^{-\bullet} \qquad k_1 = 6.5 \times 10^9\ M^{-1}s^{-1};$$

$$k_{-1} = 1.1 \times 10^5\ M^{-1}s^{-1} \qquad (24)$$

$$Cl^{\bullet} + HOCl \rightarrow H^+ + Cl^- + ClO^{\bullet} \qquad k = 3 \times 10^9\ M^{-1}s^{-1} \qquad (25)$$

$$Cl^{\bullet} + OCl^- \rightarrow Cl^- + ClO^{\bullet} \qquad k = 8.3 \times 10^9\ M^{-1}s^{-1} \qquad (26)$$

Figure 15 reflecting the synergistic effect of UV irradiation and chlorination. In this case, the free radical oxidation of ACID ORANGE 10 azo dye in chlorine photoactivated system was examinate under different initial chlorine dosage (0,1-1 mM). During the UV/TiO_2/Cl process, the initial concentration of ACID ORANGE 10 decreased rapidly, achieving up to 82% degradation within 5 min, higher than that of UV/TiO_2 alone (20%).

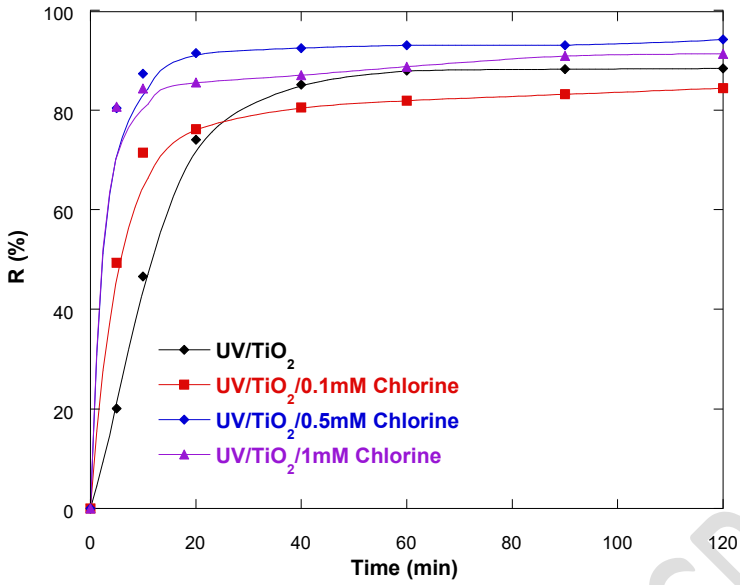

Figure 15. UV/TiO_2/Cl^- degradation system

As HOCl absorbs 254nm photons, it photolyzes into ˙OH and Cl˙. These predominant reactants significantly improve the treatment efficiency.

When chlorine concentration exceeded 1mM, decline in dye degradation was observed and the generation of RCS entered a progressive inhibition stage. However, Cl^- can scavenge •OH and Cl•, leading to the formation of dichlorine radical anion (Eq.13) which are regarded as being less reactive than Cl•. Therefore, although Cl^- classified as a radicals-scavenger (J. Díaz-Torres *et al.* 2022).

3.3.4. UV/TiO_2/IO_3^- system

iodate is considered an economical oxidant due to its better chemical stability, easy storage, and transportation safety (Renxin Li et al. 2022). To improve the degradation performance of ACID ORANGE 10, a combination between photocatalysis and periodate (PI) activation processes was performed by adding potassium periodate, leading to the production of various oxidizing species like IO˙, IO_2˙, IO_3˙, and ˙OH (M. L. Djaballah et al. 2021).

The different reactions occurring in a series of iodate photoactivation are represented as follows:

$$IO_3^- + h\nu \rightarrow IO_2^{\bullet} + O^{\bullet -} \qquad (27)$$

$$H_2O + h\upsilon \rightarrow HO^{\bullet} + H^+ \qquad (28)$$

$$IO_3^- + HO^\bullet \rightarrow IO_3^\bullet + OH^- \quad (29)$$

$$IO_3^- + IO_2^\bullet \rightarrow IO^\bullet + IO_4^- \quad (30)$$

$$HO^\bullet + HO^\bullet \rightarrow H_2O_2 \quad (31)$$

$$IO^- + HO^\bullet \rightarrow IO^\bullet + OH^- \quad (32)$$

The above mechanism shows that, a negligible production of H_2O_2 obtained from Eq.32, reflecting that H_2O_2 have not a significant role in the UV/IO_3^- oxidation system (M. L. Djaballah et al. 2021). Consequently, iodine radical intermediates ($IO^\bullet$, $IO_2^\bullet$, $IO_3^\bullet$) are the dominants species in organic pollutants degradation.

The addition of iodate (IO_3^-) significantly intensified the degradation process (Figure 16). Nearly complete ACID ORANGE 10 removal (≈97%) was achieved within 120 min, compared to 82% without iodate. Consequently, this enhancement is due to the generation of iodine-based dominants radicals ($IO^\bullet$, $IO_2^\bullet$, $IO_3^\bullet$) under UV illumination. These radicals are highly reactive oxidizing species, synergistically promoting the breakdown of the aromatic structure of ACID ORANGE 10.

Recent studies confirm iodate radicals' high redox potential (N. Guettai et al 2005). Moreover, iodate is characterized by its stability, storage and transport ability, and faster activation compared to other oxidants such as O_3, H_2O_2, and persulfate (Y. Chen et al. 2023).

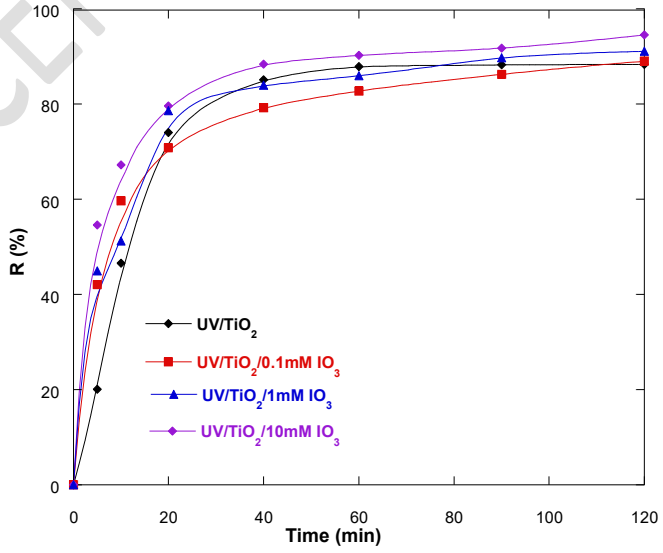

Figure 16. UV/TiO_2/IO_3^- degradation system

3.3.5. Comparative Study:

As shown in Table 3, our optimized UV/TiO_2/IO_3^- system achieves superior performance (97% removal in 120 min) compared to literature reports for similar azo dyes under UV/TiO_2 systems (typically 60-80%). More remarkably, the combination of multiple oxidants (UV/TiO_2/IO_3^-/PS) achieves 97% removal in only 5 minutes, representing a 24-fold improvement in reaction rate compared to conventional UV/TiO_2/H_2O_2 systems. This enhanced performance is attributed to the synergistic generation of multiple reactive species (•OH, $SO_4^{\bullet-}$, IO_3•) that operate through complementary oxidation pathways."

Table 3. Comparative performance of different photocatalytic systems for azo dye degradation

Study	Dye	System Conditions	Removal (%)	Time (min)
This work	Acid Orange 10	UV/TiO_2/IO_3^-, pH 6.5, 25°C	97	120
This work	Acid Orange 10	UV/TiO_2/IO_3^-/PS, pH 6.5, 25°C	97	5
Lee et al. (2023)	Orange II	UV/TiO_2 pH 3, 25°C	75	120
Zhang et al. (2024)	AO7	UV/TiO_2/H_2O_2, pH 7, 30°C	68	90
Díaz-Torres et al. (2022)	RB5	UV/TiO_2/PS pH 5, 25°C	82	120

3.3.6. Synergistic effect between oxidants

A comprehensive evaluation of ROS formation was achieved to determine the mechanism underlying the improvement in catalytic degradation compared to the ACID ORANGE 10 dye. When iodate, chlorine, persultfate and H_2O_2, entering into the system, promotes ROS generation, thereby enhancing the overall catalytic performance and confirm a strong synergistic effect between oxidants.

The observed acceleration of ACID ORANGE 10 degradation is mainly attributed to the generation of multiple reactive radicals that interact synergistically to intensify oxidation.

The comparative studies in about the two radicals $SO_4^{\bullet-}$ and $^{\bullet}OH$ found that the degradation efficiency of ACID ORANGE 10 was higher by UV/PS (88%) than that in UV/H_2O_2 (54%) in the first 5 min, which may attribute to the higher radical yield in UV/PS and stronger selectivity of $SO_4^{\bullet-}$ than $^{\bullet}OH$.

560 However, Hydroxyl radicals (•OH) have the shorter half-life with 20ns making it reacts rapidly, while
561 the sulfate radicals are much lower (20–40 μs) (Hammouda S et al 2017).
562 On the other hand, $SO_4^{\bullet-}$ could also react with Cl^- forming inorganic anion (Eq. 33), leading to the lower
563 oxidation potential in UV/H_2O_2 than that in UV/PS system.

$$SO_4^{\bullet} + Cl^- \rightarrow SO_4^{2-} + Cl^{\bullet} \qquad k = 3{,}2 \times 10^8\ M.s^{-1} \quad (33)$$

564

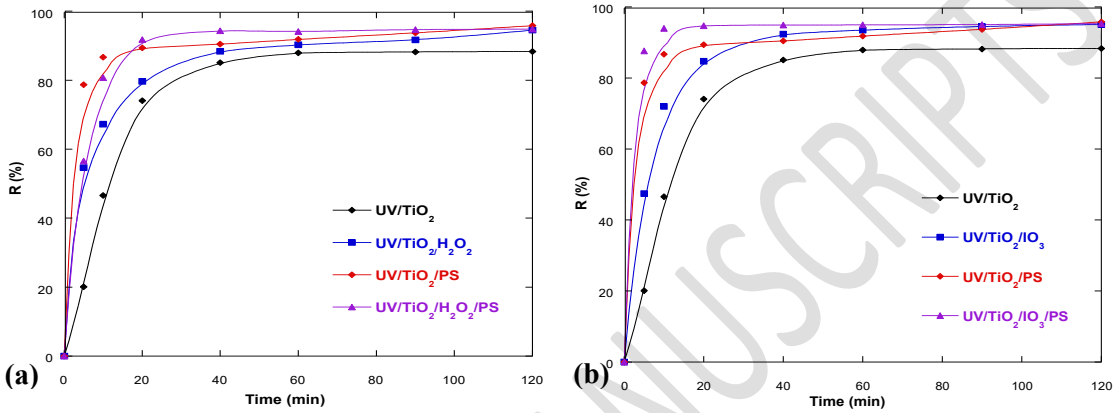

565

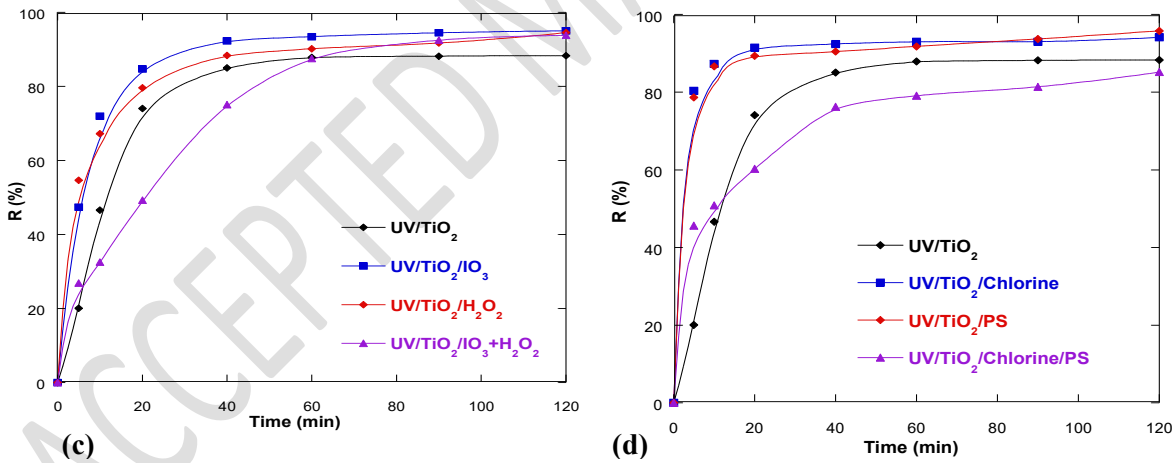

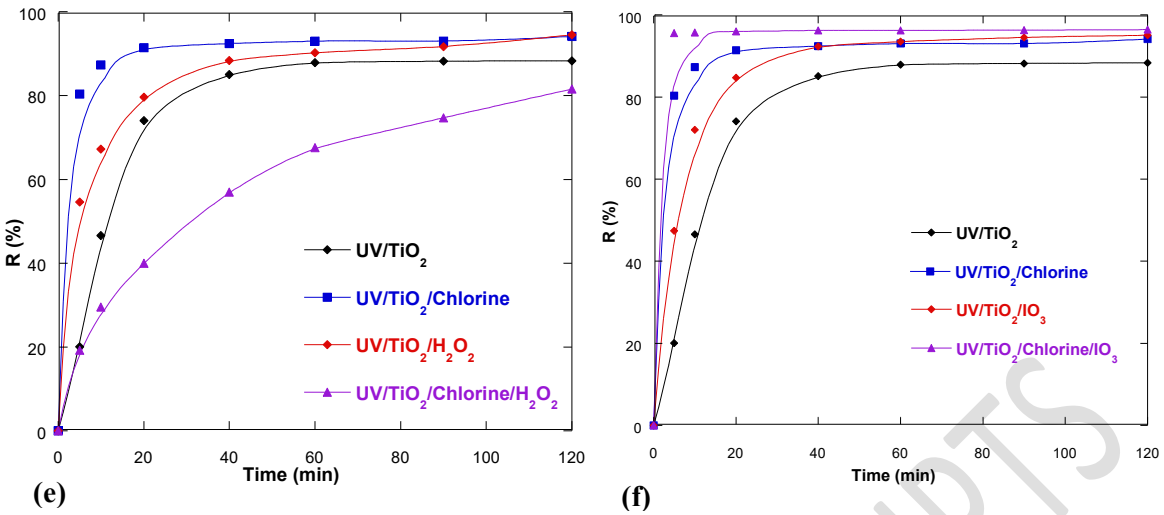

566 **Figure 17.** Comparative study of UV/TiO_2 degradation systems involving multiple oxidants:

567 (a) PS/ H_2O_2 , (b) PS/IO_3^- , (c) IO_3^-/H_2O_2 , (d) PS/ Cl^-, (e) Cl^-/H_2O_2, (f) IO_3^-/ Cl^-

568

569 Conversely, the presence of Iodine radical intermediates consistently improved performance across all

570 hybrid systems, as expressed by the trend:

571 $$UV/TiO_2/SO_4^{2-}/IO_3^- > UV/TiO_2/Cl^-/IO_3^- > UV/TiO_2/H_2O_2/IO_3^-$$

572 It should be noticed that this behavior confirms the beneficial role of iodine radicals ($IO_3^{\bullet}$, $IO_2^{\bullet}$, $IO^{\bullet}$) in

573 sustaining electron transfer and reducing charge recombination.

574 In contrast, the high values of residual H_2O_2 harm the generation of HO• and Cl• in UV/Chlorine system

575 (Eq.34) and rise HO• scavenging although producing the less reactive radical ClO•. Furthermore, the

576 generation of highly reactive species which likely acted as competitors or scavengers for radicals

577 generated during treatment limiting their availability in the solution.

$$HO^{\bullet} + Cl^- \rightarrow HClO^{\bullet} \qquad k = 4{,}3 \times 10^9\ M.s^{-1} \quad (34)$$

578

579 The synergy factor (SI) was used to evaluate the degree of intensification, confirming that the

580 combination of oxidants yields a non-linear enhancement greater than the sum of their individual effects.

581 Nearly complete mineralization (≈97%) was achieved in only 5min when all oxidizing species were

582 present simultaneously.

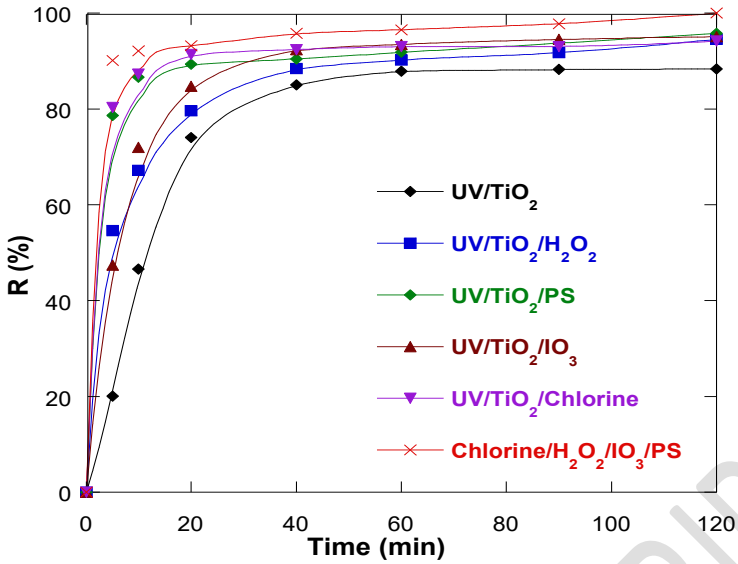

583

584 **Figure 18.** Roles of combined radicals in UV/TiO_2 system for ACID ORANGE 10 dye degradation

585

586 **3.4. Photocatalytic degradation in semi-closed system**

587 **3.4.1. Influence of inorganic and organic ions (MO and MNO)**

588 In textile effluents, dyes are often accompanied by various inorganic and organic ions that can interfere
589 with photocatalytic reactions. To evaluate this effect, different species such as KH_2PO_4, $K_4[Fe(CN)_6]$,
590 and CrK_2O_4 were introduced into the UV/TiO_2 system at concentrations ranging from 0.1 to 2 mM
591 (Figure 19).

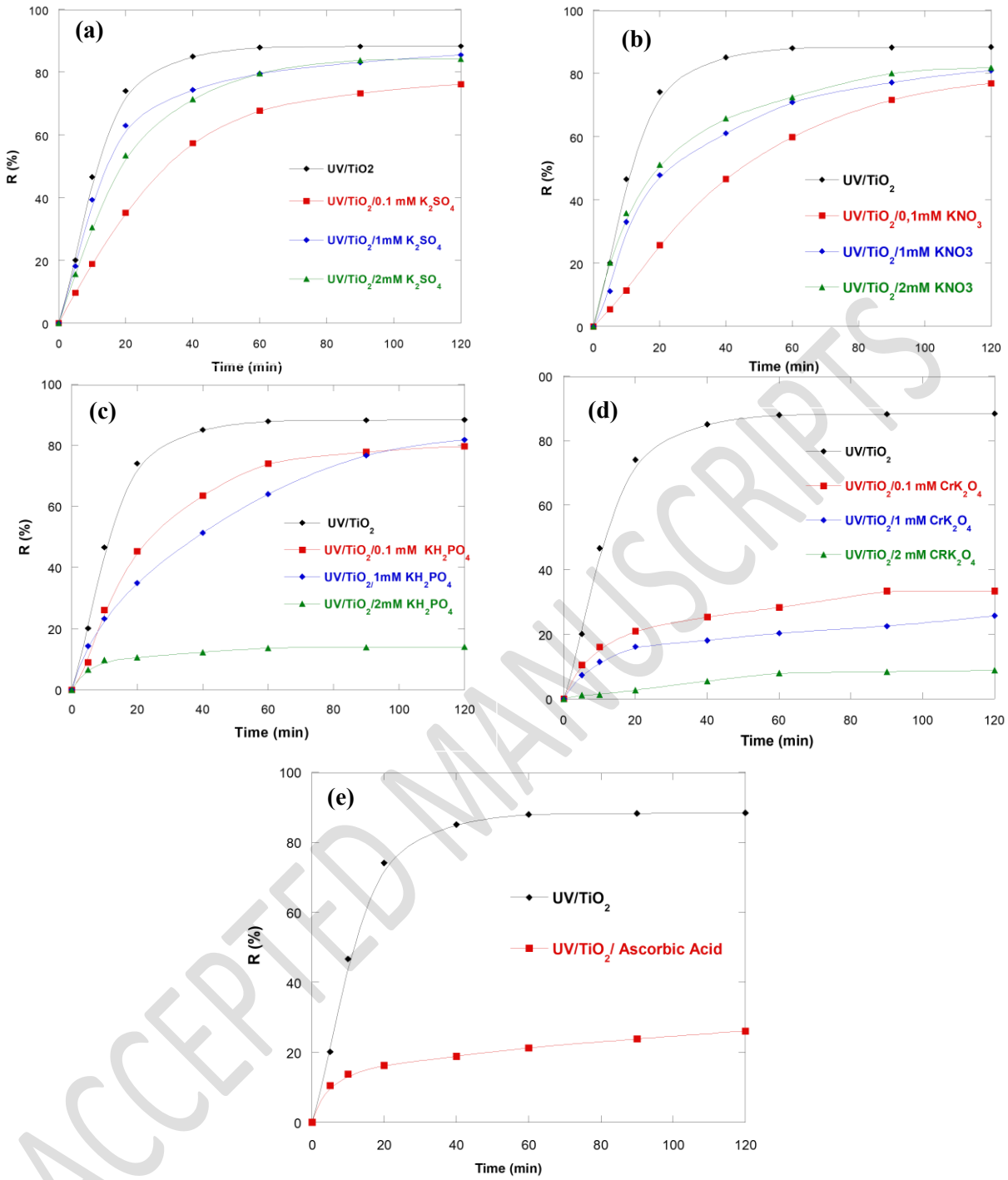

592

593 **Figure 19.** Effect of MO and MNO on the UV/TiO_2 degradation system

594 (a) UV/TiO_2/K_2SO_4, (b) UV/TiO_2/KNO_3, (c) UV/TiO_2/KH_2PO_4, (d) UV/TiO_2/Crk_2O_4,

595 (f) UV/TiO_2/ Ascorbic Acid

596

597 The results show that at low concentrations, these ions have a negligible impact on degradation

598 efficiency. However, higher concentrations lead to a marked decrease in ACID ORANGE 10 removal

due to the competitive adsorption and radical scavenging effects. Phosphate and chromate ions tend to adsorb onto the TiO_2 surface, blocking active sites and altering the surface charge, while ferrocyanide complexes can act as electron donors, reducing the formation of reactive oxygen species (ROS).

The presence of sulfate ions caused a moderate reduction in degradation rate, attributed to the formation of $SO_4^{\bullet-}$ radicals that react more slowly with ACID ORANGE 10 than hydroxyl radicals. In contrast, nitrate ions exhibited a weak promoting effect through the following photolytic reactions:

$$NO_3^- + h\nu \rightarrow NO_3^{\bullet -} \quad (35)$$

$$NO_3^{\bullet -} \rightarrow NO_2^{\bullet -} + O\ (^3P) \quad (36)$$

$$O^{\bullet -} + H_2O \rightarrow HO^{\bullet} + OH^- \quad (37)$$

$NO_2^{\bullet}$ produced by nitrate photolysis. These secondary radicals slightly enhance oxidation, suggesting that nitrate-containing matrices can partially sustain photocatalytic activity under UV irradiation.

3.4.2. Effect of alcohols

To identify the reactive species responsible for ACID ORANGE 10 degradation, alcohols such as ethanol, 2-propanol, and butanol were used as radical scavengers (Figure 20). These compounds selectively quench hydroxyl radicals (•OH) through hydrogen abstraction reactions, thereby reducing degradation efficiency.

The experimental results show a significant drop in removal efficiency from 88% (without scavenger) to 15-40% depending on the type and concentration of alcohol. This strong inhibition confirms that •OH radicals are the dominant oxidative species in the UV/TiO_2 system. Among the tested alcohols, butanol exhibited the highest quenching effect, consistent with its higher reactivity toward hydroxyl radicals (Peyton G.R et al.1988, E. Vulliet *et al.* 2003).

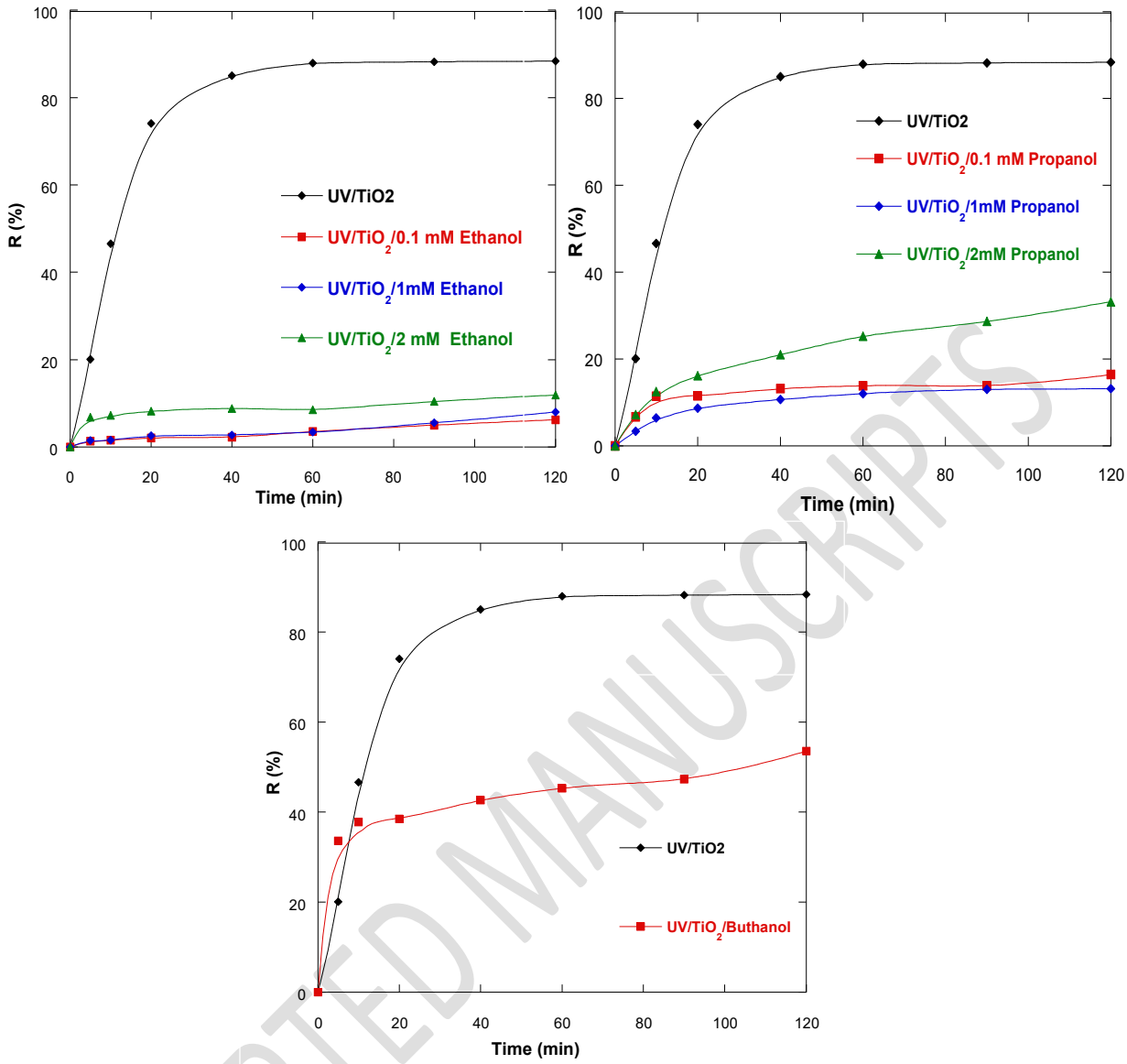

Figure 20. Influence of alcohols on the UV/TiO_2 system

3.5. Effect of real water matrices

The complexity of real wastewater, due to dissolved salts, suspended solids, dissolved organic matter, and inorganic ions, can strongly influence photocatalytic efficiency. To assess the applicability of the developed process, ACID ORANGE 10 degradation was studied using four real matrices: distilled water, river water, seawater, and mineral water (Figure 22).

The degradation performance remained high, achieving removal efficiencies of 94.5% (river water), 93.9% (seawater), and 93.6% (mineral water) within 5 min of treatment. The slight differences are

attributed to the presence of natural ions (e.g., Na^+, Mg^{2+}, Cl^-, SO_4^{2-}) that can compete for adsorption or scatter UV light. Nevertheless, the results demonstrate the robustness of the UV/TiO_2 photocatalytic process for real aqueous matrices.

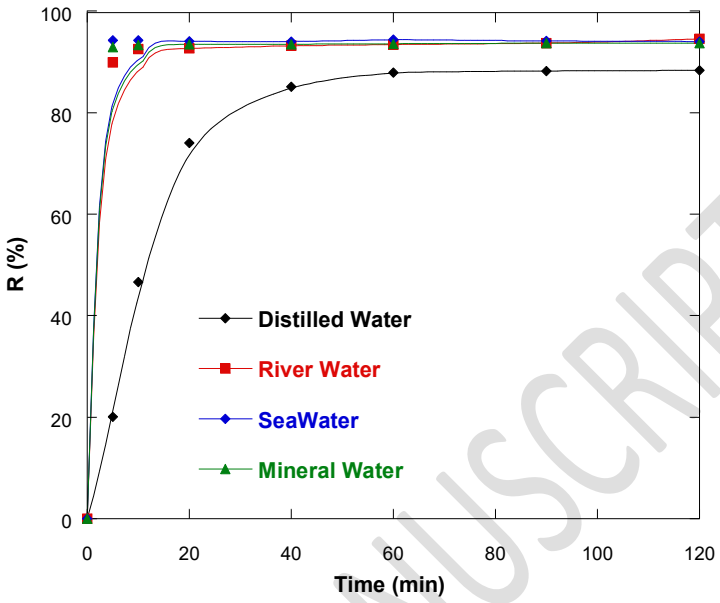

Figure 21. Effect of real matrices

These findings validate the scalability of the process for industrial wastewater treatment, particularly for textile effluents containing azo dyes such as Acid Orange 10. The combination of optimized operational parameters and oxidant-assisted intensification confirms that the system can achieve efficient, rapid, and environmentally sustainable degradation.

3.6. Comparison with Hybrid Photocatalytic Systems

Recent advances in photocatalytic technology have explored various hybrid approaches combining photocatalysis with other treatment methods or modified catalysts. Our oxidant-assisted photocatalytic system can be positioned within this broader context of hybrid technologies.

Catalyst modification approaches: Studies have reported enhanced performance through TiO_2 modification including metal doping (Ag, Cu, Fe), non-metal doping (N, S, C), and composite formation (TiO_2/graphene, TiO_2/carbon nanotubes). While these approaches improve visible light absorption and reduce electron-hole recombination, they typically require complex synthesis procedures and higher costs. In contrast, our approach of oxidant addition achieves comparable or superior performance

667 enhancement (97% removal) using commercially available TiO_2 P25 and simple oxidant addition,
668 offering practical advantages for industrial implementation (A, Rianjanu et al, 2024).
669 Process coupling approaches: Hybrid systems combining photocatalysis with electrochemical oxidation,
670 membrane filtration, or biological treatment have shown promise. However, these approaches require
671 multiple process units, complex equipment, and higher capital investment. Our semi-closed dual-reactor
672 configuration with oxidant intensification achieves similar removal efficiencies with simpler equipment
673 and operation.
674 Comparative performance: Table 4 compares our system with recently reported hybrid
675 approaches:
676 **Table 4. Performance comparison with hybrid photocatalytic systems**

System	Configuration	Removal (%)	Time (min)	Key advantage	Reference
This work	UV/TiO_2/IO_3^-/PS	97	5	Simple operation	-
Modified catalyst	UV/N-TiO_2	85	120	Visible light	(Nelson, K et al. 2024)
Photo-electro	UV/TiO_2/Electric	90	60	Higher mineralization	(Machreki, M. et al., 2023)
Photo-membrane	UV/TiO_2/UF	88	90	Continuous operation	(Bhattacharyya S et al., 2023)

677
678 Our results demonstrate that oxidant-assisted photocatalysis represents an effective and practical hybrid
679 approach that balances performance, simplicity, and cost-effectiveness for industrial wastewater
680 treatment applications.
681
682 **4. Conclusion**
683 This study demonstrates the efficiency of heterogeneous photocatalytic oxidation for degrading organic
684 pollutants in wastewater, using Acid Orange 10 as a model contaminant. The UV/TiO_2 system
685 effectively degraded the dye through hydroxyl radicals (•OH), following apparent first-order kinetics
686 under optimized conditions (10 mg/L dye, 0.1 g/L catalyst, pH ≈6.5, 25 °C).

Process intensification using external oxidants (persulfate, H_2O_2, iodate, chlorine) generated additional reactive species ($SO_4^{\bullet-}$, $Cl^{\bullet}$, $IO_3^{\bullet}$), achieving near-complete mineralization (~97%) with iodate showing the strongest synergistic effect. The system maintained high efficiency (>93%) in real water matrices (river, seawater, mineral water), confirming its applicability for complex industrial effluents.

Future work will focus on mechanistic investigations using EPR spectroscopy, development of visible-light-active catalysts, degradation pathway elucidation, ecotoxicological assessment, and pilot-scale validation under solar irradiation to enhance scalability and sustainability.

References

Abha, S., Javed, A., & Faizan, S. J. S. (2018). Application of advanced oxidation processes and toxicity assessment of transformation products. *Environmental Research*, 167, 223-233.

Aditya Rianjanua,b, et al. (2024). Integrated adsorption and photocatalytic removal of methylene blue dye from aqueous solution by hierarchical Nb2O5@PAN/PVDF/ANO composite nanofibers. *Nano Materials Science,* 6, 96–105.

Ahmad, R., et al. (2016). Photocatalytic systems as an advanced environmental remediation: Recent developments. *Journal of Environmental Chemical Engineering*, 4, 4143-4164.

Ahmed, S., Rasul, M. G., Martens, W. N., Brown, R., & Hashib, M. A. (2010). Heterogeneous photocatalytic degradation of phenols in wastewater: A review on current status and developments. *Desalination*, 261, 3-18.

Ayad, D., et al. (2024). Sustainable water production study from simulation humid air by condensation unit. *Desalination and Water Treatment*, 320. 100885

Ayad, D., et al. (2025). Synthesis and characterization of a CNT/Fe2O3/TiO2/Bentonite nanocomposite for photocatalytic degradation of tetracycline hydrochloride. *Iranian Journal of Catalysis*, Volume 15, Issue 3, 152535 (1-11).

Bhattacharyya, S., Algieri, C., Davoli, M., et al. (2023). "Polymer-based TiO_2 membranes: An efficient route for recalcitrant dye degradation". Chemical Engineering Research and Design, 194, 589-602.

Brina, R., De Battisti, A. (1987). Electrochemical methods for teaching chemistry. *Journal of Chemical Education*, 64, 175-176.

Buxton, G. V., Sellers, R. M. (1985). Radiation-induced redox reactions of iodine species. *Journal of the Chemical Society, Faraday Transactions*, 81, 475-482.

Chen, Y., et al. (2023). Insights into periodate oxidation of antibiotics mediated by visible-light-induced polymeric carbon nitride: performance and mechanism. *Chemical Engineering Journal*, 457, 141147.

Dai, M., Niu, Q. Y., Wu, S. H., Lin, Y., Biswas, J. K., Yang, C. P. (2024). Hydroxyl radicals in ozone-based advanced oxidation of organic contaminants: a review. *Environmental Chemistry Letters*, 22, 3059-3106.

Díaz-Torres, J., et al. (2022). Photocatalytic oxidation of antibiotics using transition-metal-based systems. *Applied Catalysis B: Environmental*, 320, 121879.

Díaz-Torres, J., et al. (2022). Photocatalytic removal of emerging contaminants under visible light using modified catalysts. *Applied Catalysis B: Environmental*, 320, 121879.

Djaballah, M. L., Merouani, S., Bendjama, H., Hamdaoui, O. (2021). Development of a free radical-based kinetics model for the oxidative degradation of chlorazol black using periodate photoactivated process. *Journal of Photochemistry and Photobiology A*, 408, 113102.

El-Ghenymy, A., et al. (2022). Photocatalytic degradation of dyes using TiO_2 nanomaterials. *Applied Catalysis B: Environmental*, 312, 121-139.

Furatian, L., Mohseni, M. (2018). Influence of chloride on the 185 nm advanced oxidation process. *Chemosphere*, 199, 1-8.

González-Labrada, K., et al. (2020). Enhancement of ciprofloxacin degradation by catalytic ozonation. *Environmental Science and Pollution Research*, 27, 1246-1255.

Guettai, N., Amar, H. A. (2005). Photocatalytic degradation of azo dyes. *Desalination*, 185, 427-438.

Guettai, N., Amar, H. A. (2005). Photocatalytic degradation of methyl orange in aqueous TiO_2 suspension. *Desalination*, 185, 427-438.

Hammouda, S. B., et al. (2017). Degradation and mineralization of phenol in aqueous medium by heterogeneous monopersulfate activation on nanostructured cobalt-based perovskite catalysts $ACoO_3$. *Applied Catalysis B: Environmental*, 215, 60-73.

Hao, P. L., Hu, M. Z., Xing, R., Zhou, W. J. (2020). Synergistic degradation of methylparaben on $CuFe_2O_4$-rGO composite by persulfate activation. *Journal of Alloys and Compounds*, 823, 153757.

Hoffmann, M. R., Martin, S. T., Choi, W., & Bahnemann, D. W. (2022). Environmental applications of semiconductor photocatalysis. *Chemical Reviews*, 95, 69–96.

Ike, I. A., Linden, K. G., Orbella, J. D., & Duke, M. (2018). Critical review of the science and sustainability of persulphate advanced oxidation processes. *Chemical Engineering Journal*, 338, 651-669.

Karuppaiah, S., et al. (2019). Photocatalytic degradation of bisphenol A using ZnO/bentonite nanocomposite. *Applied Surface Science*, 481, 1109-1119.

Kumar, S., et al. (2023). "A review on photocatalysis used for wastewater treatment: dye degradation". Water, Air, & Soil Pollution, 234, 280.Lee, C., et al. (2023). Degradation of organic pollutants using advanced oxidation processes: mechanisms and kinetics. *Journal of Environmental Chemical Engineering*, 11, 110807.

Legrini, O., Oliveros, E., & Braun, A. M. (1993). Photochemical processes for water treatment. *Chemical Reviews*, 93, 671-698.

759 Li, R., Wang, J., Han, W., Zhu, Z., & Guo, H. (2022). Periodate activation for degradation of organic
760 contaminants: processes, performance and mechanism. *Separation and Purification*
761 *Technology*, 292, 120928.

762 Li, S., et al. (2023). Antibiotics degradation by advanced oxidation process: ecotoxicity and antibiotic-
763 resistance genes induction. *Chemosphere*, 311, 136977.

764 Lin, Y., Ferronato, C., Deng, N., Wu, F., Chovelon, J.-M. (2009). Photocatalytic degradation of
765 methylparaben by TiO_2: multivariable experimental design and mechanism. *Applied Catalysis*
766 *B: Environmental*, 88, 32-41.

767 Lu, Z., et al. (2022). Antibiotics degradation by UV/chlorine advanced oxidation processes: A
768 comprehensive review. *Environmental Pollution*, 308, 119673.

769 Machreki, M., Chouki, T., Tyuliev, G., et al. (2023). "Defective TiO_2 Nanotube Arrays for Efficient
770 Photoelectrochemical Degradation of Organic Pollutants". ACS Omega, 8(15), 14066-14077.

771 Mohod, A. V., Teixeira, A. C. S. C., Bagal, M. V., Gogate, P. R., Giudici, R. (2023). Degradation of
772 organic pollutants from wastewater using hydrodynamic cavitation: a review. *Journal of*
773 *Environmental Chemical Engineering*, 11, 109773.

774 Mohammed J. A., et al. (2025). Effective adsorption of Chromium (III) ions from the tannery effluent
775 wastewater using Cerium Oxide (CeO2) nanoparticles. *Indian Chemical Engineer*, Online, 1-
776 18.

777 Nelson, K., Mecha, A.C., & Kumar, A. (2024). "Characterization of novel solar based nitrogen doped
778 titanium dioxide photocatalytic membrane for wastewater treatment". Heliyon, 10(9), e29806.

779 Oller, I., Malato, S., & Sánchez-Pérez, J. A. (2011). Combination of advanced oxidation processes and
780 biological treatments for wastewater decontamination: A review. *Science of the Total*
781 *Environment*, 409, 4141-4166.

Peng, L., Yuan, Y., Wang, Z., Wang, W., & Wu, Q. (2024). Iron single atoms anchored on ultrathin carbon nitride photocatalyst for visible-light water decontamination. *Journal of Hazardous Materials*, 474, 134703.

Peyton, G. R., & Glaze, W. H. (1988). Destruction of pollutants with ozone/UV: photolysis of aqueous ozone. *Environmental Science & Technology*, 22, 761–767.

Rook, J. J. (1974). Formation of haloforms during chlorination of natural waters. *Water Treatment and Examination*, 23, 234-241.

Samadi, M., Zirak, M., Naseri, A., Khorashadizade, E., & Moshfegh, A. Z. (2016). Fabrication and characterization of ZnO nanostructures for photocatalytic applications. *Thin Solid Films*, 605, 19-26.

Sivasubramanian S, Gopalsamy Venkatesan SK, Thanarajan T, Rajendran S. (2025). Al-Biruni Earth Radius Optimization for enhanced environmental data analysis in remote sensing imagery. *Agrociencia*. Vol 59i5.3380.

Sleiman, M., Conchon, P., Ferronato, C., & Chovelon, J.-M. (2009). Photocatalytic oxidation of toluene at indoor air levels. *Applied Catalysis B: Environmental*, 86, 159–165.

Suty, H., de Traversay, C., Coste, M. (2021). Application of AOPs: Present and future. *Water Science and Technology*, 8, 12-23.

Venkatraman M., Surendran R., Srinivasulu S. Vijayakumar K. (2024). Water quality prediction and classification using Attention based Deep Differential Recur Flow Net with Logistic Giant Armadillo Optimization", *Global NEST*, Vol 27, No 1, 06799.

Vulliet, E., Chovelon, J.-M., Guillard, C., & Herrmann, J.-M. (2003). Factors influencing the photocatalytic degradation of sulfonylurea herbicides by TiO_2. *Journal of Photochemistry and Photobiology A*, 159, 71-79.

Wang, Y. R., et al. (2019). Nanoscaled magnetic $CuFe_2O_4$ as an activator of PMS for norfloxacin degradation. *Separation and Purification Technology*, 212, 536-544.

Wang, H. J., et al. (2025). Controlled construction of single-atom iron for pollutant elimination. *Chemical Engineering Journal*, 516, 164113.

Wu, T., Liu, G., Zhao, J., Hidaka, H., Serpone, N. (1998). Self-photosensitized oxidative transformation of Rhodamine B. *Journal of Physical Chemistry B*, 102, 5845–5851.

Yang, Q., et al. (2019). Recent advances in photo-activated sulfate radical-AOP for refractory organic pollutants. *Chemical Engineering Journal*, 378, 122149.

Yudha Gusti Wibowoa, et al. (2025). Biochar-layered double hydroxide vs biochar-layered double oxide: a critical review on their applications in water pollution control. *Water-Energy Nexus,* 8, 205–228

Zadvarzi, S. B., Khavarpour, M., Vahdat, S. M., Baghbanian, S. M., & Rad, A. S. (2021). Fe_3O_4@chitosan@ZIF-8 for removal of malachite green. *International Journal of Biological Macromolecules*, 168, 428-441.

Zaviska, F., Drogui, P., Mercier, G., Blais, J. (2009). Advanced oxidation processes in water treatment: A review. *Environmental Technology*, 30, 1101-1110.

Zhang, L., et al. (2024). Degradation of dyes in aqueous media via sulfate radical AOP. *Chemosphere*, 352, 140221.

Zhang, X., Duan, X., Sun, H., Wang, S. (2019). Activation of persulfate by transition metals for organic pollutant degradation. *Chemical Engineering Journal*, 370, 1167-1180.

Zhang, X., Yu, X., Kamali, M., Appels, L., Van der Bruggen, B., Cabooter, D., Dewil, R. (2021). Efficiency and mechanism of 2,4-dichlorophenol degradation by UV/IO_4^-. *Science of the Total Environment*, 782, 146781.

Zhao, Y., et al. (2020). Scavenging of pharmaceuticals by activated carbon fiber. *Chemosphere*, 247, 1259.

Zhu, Z., Zhao, X., Xiao, X., Xu, C., Zuo, X., Nan, J. (2022). Formation of surface oxygen vacancies in Bi-based hybrid photocatalyst. *Journal of Colloid and Interface Science*, 625, 109-118.